

Research Article

Open Access



Energy storage properties of NaNbO_3 -based lead-free superparaelectrics with large antiferrodistortion

Guanfu Liu, Liang Chen, He Qi

Beijing Advanced Innovation Center for Materials Genome Engineering, Department of Physical Chemistry, University of Science and Technology Beijing, Beijing 100083, China.

Correspondence to: Prof./Dr. He Qi, Beijing Advanced Innovation Center for Materials Genome Engineering, Department of Physical Chemistry, University of Science and Technology Beijing, No. 30 Xueyuan Road, Haidian District, Beijing 100083, China. E-mail: qiheustb@ustb.edu.cn

How to cite this article: Liu G, Chen L, Qi H. Energy storage properties of NaNbO_3 -based lead-free superparaelectrics with large antiferrodistortion. *Microstructures* 2023;3:2023009. <https://dx.doi.org/10.20517/microstructures.2022.29>

Received: 25 Sep 2022 **First Decision:** 7 Nov 2022 **Revised:** 28 Nov 2022 **Accepted:** 26 Dec 2022 **Published:** 12 Jan 2023

Academic Editors: Zhihua Sun, Ruzhong Zuo **Copy Editor:** Fangling Lan **Production Editor:** Fangling Lan

Abstract

NaNbO_3 -based lead-free energy storage ceramics are essential candidates for next-generation pulsed power capacitors, especially under the background of energy saving and environmental protection. However, the room-temperature antiferroelectric P phase of pure NaNbO_3 ceramics limits its further development in energy storage owing to the irreversible antiferroelectric to ferroelectric phase transition under electric fields. In this work, CaZrO_3 was introduced to NaNbO_3 ceramics to destroy the long-range polarization ordering but keep large antiferrodistortion, causing the formation of superparaelectric state with macrodomains, which can be identified by the refinement results of high-energy synchrotron X-ray diffraction, neutron diffraction and TEM results. Combined with the fine grains, dense and homogeneous microstructure, ergodic relaxation behaviors, and delayed polarization saturation, a high recoverable energy storage density of $\sim 5.4 \text{ J/cm}^3$ and efficiency of $\sim 82\%$ can be realized in $0.85\text{NaNbO}_3\text{-}0.15\text{CaZrO}_3$ ceramics at an ultrahigh breakdown electric field of $\sim 68 \text{ kV/mm}$. The results found in this work suggest that the supersparaelectric with non-cubic phase would be a good candidate for generating excellent dielectric energy storage properties.

Keywords: NaNbO_3 , energy storage, relaxor ferroelectric, oxygen octahedral distortion

INTRODUCTION

Energy plays an irreplaceable role in the development of human society, and how to efficiently store energy



© The Author(s) 2023. **Open Access** This article is licensed under a Creative Commons Attribution 4.0 International License (<https://creativecommons.org/licenses/by/4.0/>), which permits unrestricted use, sharing, adaptation, distribution and reproduction in any medium or format, for any purpose, even commercially, as long as you give appropriate credit to the original author(s) and the source, provide a link to the Creative Commons license, and indicate if changes were made.



has gradually become the focus of research. Currently, energy storage devices are mainly divided into four categories: lithium-ion batteries, fuel cells, electrochemical super-capacitors, and dielectric capacitors^[1-3]. Solid-state dielectric capacitors, compared with other energy storage devices, possess high power density and ultrafast charge-discharge rates, which are widely used in advanced high power and pulse power electronic devices, such as hybrid electric vehicles, distributed power systems, and directional energy weapons^[4,5]. However, the low recoverable energy storage density (W_{rec}) limits their energy storage development.

In the context of energy saving and environmental protection, to effectively improve the W_{rec} of dielectric capacitors, lead-free perovskite energy storage ceramics have become a research hotspot^[6,7]. The total energy storage density (W_{total}), W_{rec} , and efficiency (η) are the main parameters to evaluate energy storage performance which can be calculated based on the following formula:

$$W_{rec} = \int_{P_r}^{P_{max}} E dP \quad (1)$$

$$W_{total} = \int_0^{P_{max}} E dP \quad (2)$$

$$\eta = \frac{W_{rec}}{W_{total}} \quad (3)$$

where P_{max} , P_r , and E are the maximum polarization, remanent polarization, and applied electric field, respectively. As a result, large ΔP ($P_{max}-P_r$) and high E_b are indispensable for materials with high W_{rec} ^[8]. The researches on lead-free energy storage materials generally focus on linear dielectrics, ferroelectrics, antiferroelectrics, and relaxor ferroelectrics. Linear dielectrics possess ultrahigh η and E_b but low W_{rec} due to their low polarization characteristic^[9]. Both high P_{max} and P_r can be found in ferroelectrics, resulting in highly inferior W_{rec} and η . Similarly, antiferroelectrics also own unsatisfactory energy storage properties with low η and poor cycle stability because of irreversible antiferroelectric to ferroelectric phase transition under applied electric field and comparatively significant difference between E_F and E_A ^[10-12]. Relaxor ferroelectrics are characterized by a diffuse phase transition over a broad temperature range, from the Burns temperature (T_B) at which nanodomains appear, to the intermediate temperature (T_m) at which nanodomains grow and the permittivity reaches the maximum, and finally to the freezing temperature (T_f) at which nanodomains become frozen ($T_f < T_m < T_B$)^[13,14]. In particular, relaxor ferroelectrics located at the temperature range of T_m-T_B can be defined as superparaelectrics, in which the size of nanodomains is further decreased, and the domain interaction is further weakened^[14]. Therefore, Relaxor ferroelectrics, especially for superparaelectrics^[15,16], show excellent performance superiority for achieving both high W_{rec} and η simultaneously^[17-20].

NaNbO_3 (NN) is one of the typical lead-free ferroelectrics with complex crystal structure and phase transition under various temperatures. Despite the remaining controversies, it is commonly agreed that NN adopts seven major phases with the sequence of $U \rightarrow T_2 \rightarrow T_1 \rightarrow S \rightarrow R \rightarrow P \rightarrow N$ on cooling, where the common P and R phases are antiferroelectrics^[21,22]. The complex temperature-driven structure also means great potential for performance regulation. NN ceramic exhibits antiferroelectric P phase structure with P6mm space group at room temperature^[23,24]. Generally, an effective strategy to improve the energy storage of NN ceramics focuses on stabilizing their antiferroelectric phase. For example, ultrahigh W_{rec} of 12.2 J/cm^3 was obtained in $0.76\text{NaNbO}_3-0.24(\text{Bi}_{0.5}\text{N}_{0.5})\text{TiO}_3$ ceramics due to stable relaxor antiferroelectric phase, however,

accompanied by a relatively low η of 69% owing to large polarization hysteresis for the first-order antiferroelectric-ferroelectric phase transition under high electric field^[25]. Therefore, a practical approach is urgently required to simultaneously regulate the W_{rec} and η of NN ceramics. In this work, CaZrO₃ (CZ) was introduced into NN ceramics to not only destroy long-range antiferroelectric ordering but also remain large antiferrodistortion. On the one hand, the enhanced local random field along with the strengthened dielectric relaxation behavior would benefit the high η owing to the fast response of nanoclusters to the external electric field. On the other hand, the existence of large oxygen octahedron tilt would hinder the formation of long-range ferroelectric ordering under electric field, leading to the delayed polarization saturation process. Combined with the fine grains, dense and homogeneous microstructure, ergodic relaxation behavior, and delayed polarization saturation, a high recoverable energy storage density of ~ 5.4 J/cm³ and a large efficiency of $\sim 82\%$ can be realized in 0.85NaNbO₃-0.15CaZrO₃ ceramics at an ultrahigh breakdown electric field of ~ 68 kV/mm, showing a great application potential in the field of dielectric energy storage.

MATERIALS AND METHODS

Sample preparation

The ceramics of (1- x)NaNbO₃- x CaZrO₃ ((1- x)NN- x CZ, $x = 0-0.15$) were prepared by the conventional solid-state reaction process. The raw materials of Na₂CO₃ (> 99.9%), CaCO₃ (> 99.5%), Nb₂O₅ (> 99.9%), and ZrO₂ (> 99.9%) were weighed according to the chemical formula and mixed by planetary ball milling for 8 h using ethanol as ball milling media. The mixed powders were calcined at 850 °C for 5 h after drying. Then, the calcined powders were ball-milled again by high-energy ball milling (700 r/min for 8 h) with ethanol and 0.5 wt% PVB binder. Afterward, the powders were pressed into pellets with a diameter of 8 mm and a thickness of ~ 1 mm. The pellets were sheathed using the corresponding calcined powders in crucibles and sintered at 1370 °C for 2 h. Finally, the sintered ceramics were polished to a thickness of ~ 0.1 mm with a diameter of ~ 6.5 mm and coated with silver electrodes with a diameter of ~ 2 mm, which were fired under 550 °C for 30 min to measure their electrical properties.

Structural and performance characterizations

The high-energy synchrotron X-ray diffraction (SXRD) data was measured on the 11-ID-C beamline of advanced photon source. Powder neutron diffraction data were collected at CSNS (China Spallation Neutron Source, MPI) using time-of-flight powder diffractometers. The diffraction data refinement was taken by the Rietveld method on software GSAS II. Temperature- and frequency-dependent dielectric properties were carried out using an impedance analyzer (Keysight E4990A, Santa Clara, CA). Domain morphology and selected area electron diffraction (SAED) were observed on a field-emission transmission electron microscope (TEM, JEM-F200, JEOL, Japan) at an accelerating voltage of 200 kV. High-angle annular dark-field (HAADF) atomic-scale images were obtained using an atomic-resolution scanning transmission microscope (STEM, aberration-corrected Titan Themis 3300), and the polarization vectors, polarization magnitude, and polarization angle maps were calculated by customized MATLAB scripts. The morphology of grains was filmed using a scanning electron microscope (SEM, LEO1530, ZEISS SUPRA 55, Oberkochen, Germany). Energy-storage properties of ceramics were investigated by a ferroelectric analyzer (aix ACCT, TF Analyzer 1000, Aachen, Germany).

RESULTS AND DISCUSSION

Figure 1A shows the temperature-dependent dielectric permittivity (ϵ_r) of (1- x)NN- x CZ ceramics at 1 MHz. Pure NN is determined to be antiferroelectric P phase structure at room temperature accompanied by two dielectric anomaly peaks at 130 °C and 370 °C, representing the transitions from antiferroelectric P phase to incommensurate (INC) phase and INC phase to antiferroelectric R phase, respectively^[26-28]. With the

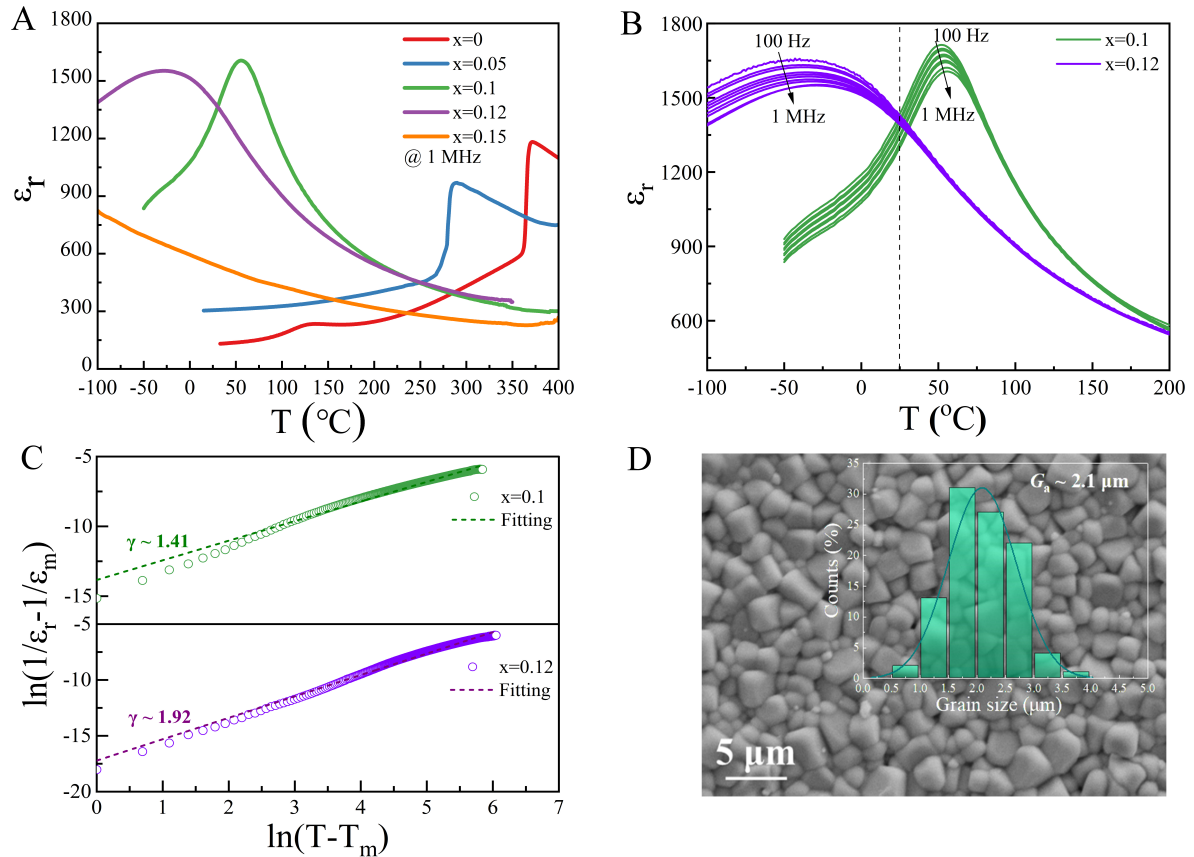


Figure 1. (A) Temperature-dependent dielectric permittivity for (1-x)NN-xCZ ceramics. (B) Frequency-dependent dielectric permittivity and (C) diffuseness degree (γ) fitted from the modified Curie-Weiss law for $x = 0.1$ and 0.12 . (D) SEM surface morphology and grain size distribution of $0.85\text{NN}-0.15\text{CZ}$ ceramic.

increase of CZ, the dielectric anomaly peak at 130°C disappears, and the maximum dielectric peak shifts gradually to low temperature together with the transition of phase structure. To characterize the relaxor feature, the dielectric properties of $x = 0.1$ and 0.12 at different frequencies are shown in [Figure 1B](#). Both samples exhibit apparent frequency dispersion behavior. As shown in [Figure 1C](#), the diffuseness degree (γ) for $x = 0.1$ and 0.12 was obtained using the modified *Curie-Weiss* Law:

$$\frac{1}{\epsilon_r} - \frac{1}{\epsilon_m} = \frac{(T - T_m)^\gamma}{C} \quad (T > T_m) \quad (4)$$

where ϵ_m is the maximum dielectric permittivity and T_m is the according temperature, C is the Curie constant. The γ value of $0.9\text{NN}-0.1\text{CZ}$ and $0.88\text{NN}-0.12\text{CZ}$ ceramics are ~ 1.41 and ~ 1.92 , respectively, indicating that the (1-x)NN-xCZ ceramics should be relaxor ferroelectrics for $x \geq 0.1$. These also demonstrate that the Ca^{2+} and Zr^{4+} are substituted into the lattice of NN matrix, breaking the long-range antiferroelectric order and increasing the local random field. Especially, the relaxed dielectric peak of $0.85\text{NN}-0.15\text{CZ}$ ceramic located far below room temperature and the $T_B \sim 85^\circ\text{C}$ obtained according to the *Curie-Weiss* Law, as shown in [Supplementary Figure 1](#), indicate it should be superparaelectric state around room temperature. It is recognized that ultrasmall and highly active polar nanoregions (PNRs) can be found in the superparaelectric region, leading to the improvement of η ^[29-31]. Compared with other samples, $0.85\text{NN}-0.15\text{CZ}$ ceramic has moderate room-temperature $\epsilon_r \sim 545$, which can effectively delay the

polarization saturation process under a low electric field and reduce the possibility of electromechanical breakdown generated by the electrostriction effect. These phenomena indicate that 0.85NN-0.15CZ ceramic shows excellent potential to become a high energy storage material.

Another basic guarantee for realizing high energy storage properties is the uniform and compact microstructure. As shown in [Figure 1D](#), the surface morphology of 0.85NN-0.15CZ ceramic presents a dense microstructure with few pores. A uniform grain size distribution can be found in 0.85NN-0.15CZ ceramic with a smaller average grain size (G_a) of $\sim 2.1 \mu\text{m}$ compared with that of pure NN ceramic shown in [Supplementary Figure 2](#). Moreover, the uniform distribution of elements in [Supplementary Figure 3](#) suggests the achievement of a pure phase structure. It is believed that good sample quality, along with small grain size and dense structure, is beneficial to strengthening E_b .

Even though a superparaelectric state for the 0.85NN-0.15CZ ceramic can be easily identified by using dielectric spectra, however, it is widely known that there are several different paraelectric states as well as (anti)ferroelectric states in NN ceramics at different temperature ranges. To analyze the phase structure of 0.85NN-0.15CZ ceramic, as shown in [Figure 2A](#) and [B](#), high-energy SXRD and powder neutron diffraction data were collected and refined. Together with the EDS images shown in [Supplementary Figure 3](#), the sample should certainly be a pure perovskite phase. Moreover, apparent non-cubic phase structure can be identified for 0.85NN-0.15CZ ceramic according to the split main diffraction peaks and superlattice diffraction peaks. This feature is quite different from the average structure characteristics of traditional superparaelectrics^[15,16], indicating the existence of lattice distortion. The lattice distortion in (anti)ferroelectrics mainly includes oxygen octahedron tilt and cation off-centering displacement. Considering the macro nonpolar feature of superparaelectrics, the lattice distortion in the studied sample should be attributed to the oxygen octahedron tilt. As the insensitive response of X-ray to the oxygen ions, powder neutron diffraction was measured. Rietveld refinement using the model with $P2_1ma$ space group was taken simultaneously on the SXRD and neutron diffractions, and the satisfying results with low-reliability factors of weighted patterns (R_{wp}) are shown in [Figure 2A](#) and [B](#). To convince the best refinement result, Rietveld refinement of SXRD data using the model with cubic space group of $Pm-3m$ was also carried out in [Supplementary Figure 4](#). It can be found that the 0.85NN-0.15CZ ceramic should be a ferroelectric Q phase with $P2_1ma$ space group and $a'b^+c^-$ oxygen octahedron tilt system but small polarization displacement, which is different from that of NN ceramic (P phase: $a'b^+c^-/a'b^+c^-$). According to Glazer notation, the superscripts +, -, and 0 represent in-phase tilt, anti-phase tilt, and no tilt of oxygen octahedron along one axis, respectively^[32]. The tilt degree of oxygen octahedron can be calculated using $\omega = (180^\circ - \angle B-O-B)/2$. As shown in [Supplementary Figure 5](#), the oxygen octahedron tilt degree for NN ceramics with $Pbcm$ space group at room temperature is calculated as $\sim 7.9^\circ$ - 13.15° . According to the lattice parameters obtained from the refinement results of SXRD and powder neutron diffraction, the crystal structure model of 0.85NN-0.15CZ ceramic was drawn and displayed in [Figure 2C](#). A large oxygen octahedron tilt of $\sim 10.89^\circ$ - 12.20° can be calculated according to the $\angle B-O1-B \sim 157.55^\circ$, $\angle B-O2-B \sim 156.61^\circ$, $\angle B-O3-B \sim 155.61^\circ$, and $\angle B-O4-B \sim 158.22^\circ$, which is much larger than that of traditional relaxor ferroelectrics such as $\text{Pb}(\text{Mg}_{1/3}\text{Nb}_{2/3})\text{O}_3$ and $\text{Ba}(\text{Ti}, \text{Zr})\text{O}_3$. That is to say, the relaxor ferroelectric Q phase can be identified in 0.85NN-0.15CZ ceramic, which is quite different from the previously reported results that the addition of CZ would stabilize antiferroelectric P phase in NN ceramic^[33-35]. The decreased tolerance factor after doping CZ into NN ceramic would increase the oxygen octahedron tilt. However, according to the statistics of recently reported antiferroelectrics (NN, AgNbO_3 , $(\text{Bi}_{0.5}\text{Na}_{0.5})\text{TiO}_3$ -based, BiFeO_3 -based, PbZrO_3 , and PbHfO_3 -based ceramics), it can be found that the antiferroelectric phase only exists in a narrow tolerance factor range. The perovskites with ultralow tolerance factor are usually paraelectrics, such as CaZrO_3 and CaHfO_3 . Therefore, the polarization ordering would be destroyed when the amount of CZ is over a critical value, leading to the

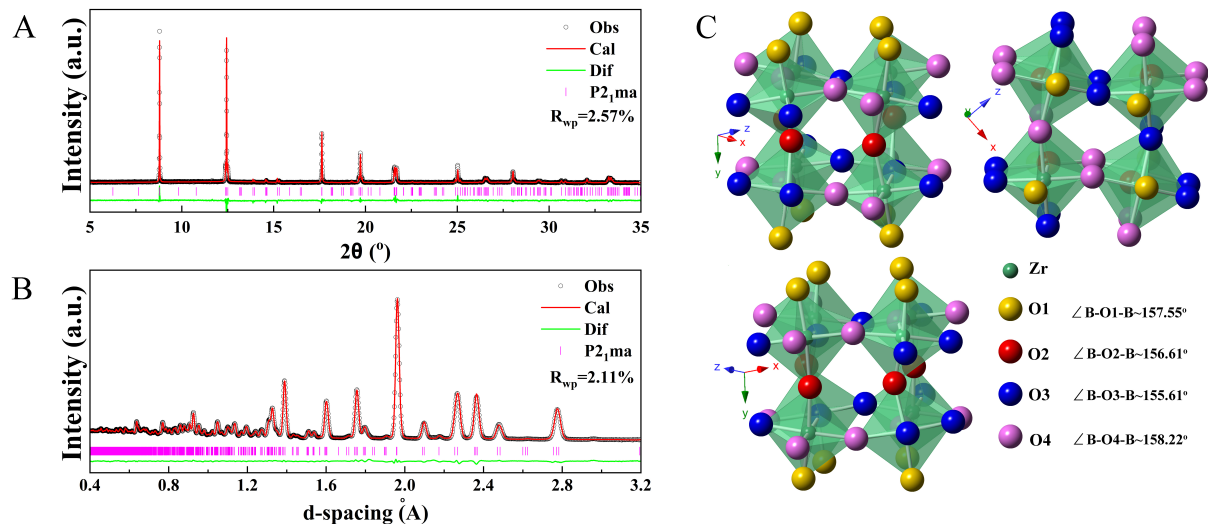


Figure 2. (A) High-energy synchrotron XRD, and (B) powder neutron diffraction structure refinement patterns of 0.85NN-0.15CZ Ceramic. (C) Schematic diagram of the large antiferrodistortion in 0.85NN-0.15CZ ceramic.

disappearance of anti-phase tilt modules along b axis. Moreover, the formation of dielectric relaxation behavior would also destroy the long-range polarization ordering. As a result, a superparaelectric state with large antiferrodistortion can be detected in 0.85NN-0.15CZ ceramic at room temperature.

TEM is an essential and helpful method to characterize the domain morphology and lattice microstructure for ferroelectric materials. [Figure 3A](#) suggests that 0.85NN-0.15CZ ceramic exhibits apparent 90° and 180° microdomains. [Figure 3B](#) and [C](#) display high-resolution TEM lattice fringe images along $[100]_c$ and $[111]_c$ directions, respectively, demonstrating good sample quality. [Figure 3D](#) and [E](#) show the SAED image along $[100]_c$ and $[111]_c$ directions, respectively, which once again confirm that 0.85NN-0.15CZ ceramic should be pure perovskite structure. It is recognized that the $1/2$ types of superlattice diffractions of $(0oe)/2$ and $(ooo)/2$ (o and e are odd and even, respectively) are mainly related to the in-phase and anti-phase oxygen octahedron tilt, respectively^[32]. Therefore, the $1/2$ type superlattice diffraction spots observed in the accordingly SAED images further prove the existence of oxygen octahedral distortion. It is widely accepted that normal ferroelectrics with macrodomains exhibit poor energy storage properties ascribed to the large polarization hysteresis along with irreversible domain switching, which occurs together with polarization reorientation. However, there is no macroscopic polarization alignment in this superparaelectric sample, which could be further directly confirmed by the quantitative analysis of the polarization mapping using HAADF-STEM results, as shown in [Figure 4](#). Therefore, these macrodomains should be ferroelastic domains constructed by the ordered oxygen octahedron tilt, and the domain switching process has very little influence on polarization reorientation. According to the polarization mapping, ultrasmall PNRs with a size of about 2-3 nm can be seen, which is at the same level as other superparaelectrics. Namely, fast response of PNRs with little polarization hysteresis during charging and discharging processes can also be expected for this sample, benefiting excellent energy storage properties. Moreover, large antiferrodistortion would also delay the polarization saturation process, which would also favor the energy storage properties.

Due to the irreversible phase transition from antiferroelectric to ferroelectric under electric fields for pure NN ceramic, a square P-E loop with poor energy storage properties can be achieved, as shown in [Supplementary Figure 6](#). With the stabilization of antiferroelectric P phase by adding a small content of CZ^[35], even though increased energy storage density can be obtained along with the appearance of

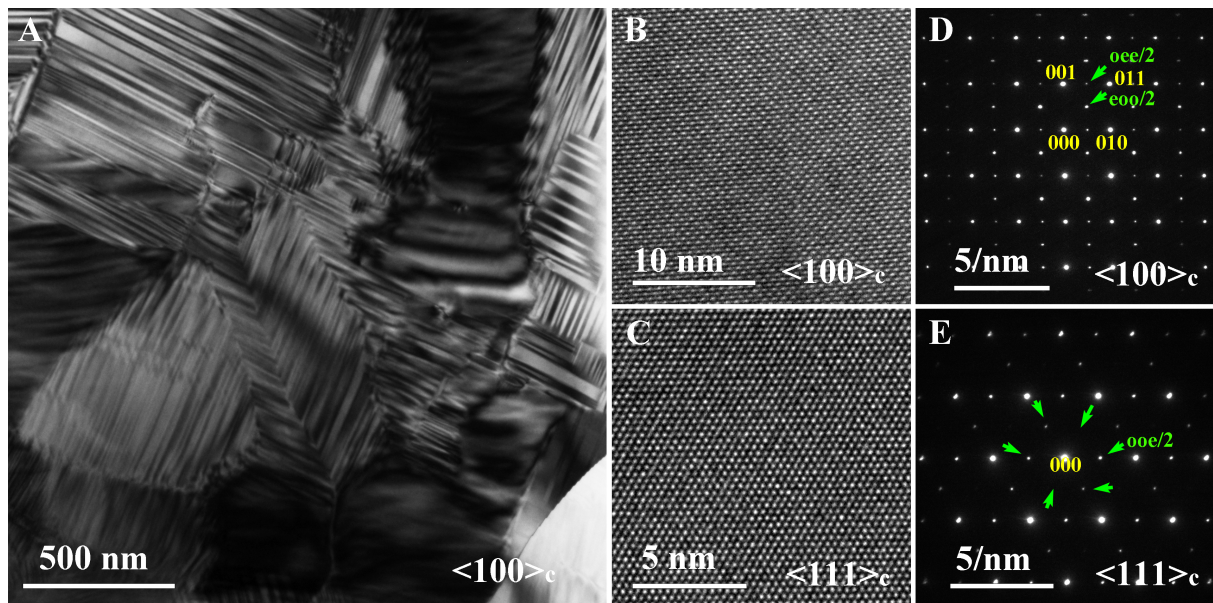


Figure 3. (A) Domain morphology of 0.85NN-0.15CZ ceramic. Lattice fringes and SAED patterns of 0.85NN-0.15CZ ceramic along (B and D) $[100]_c$ and (C and E) $[111]_c$.

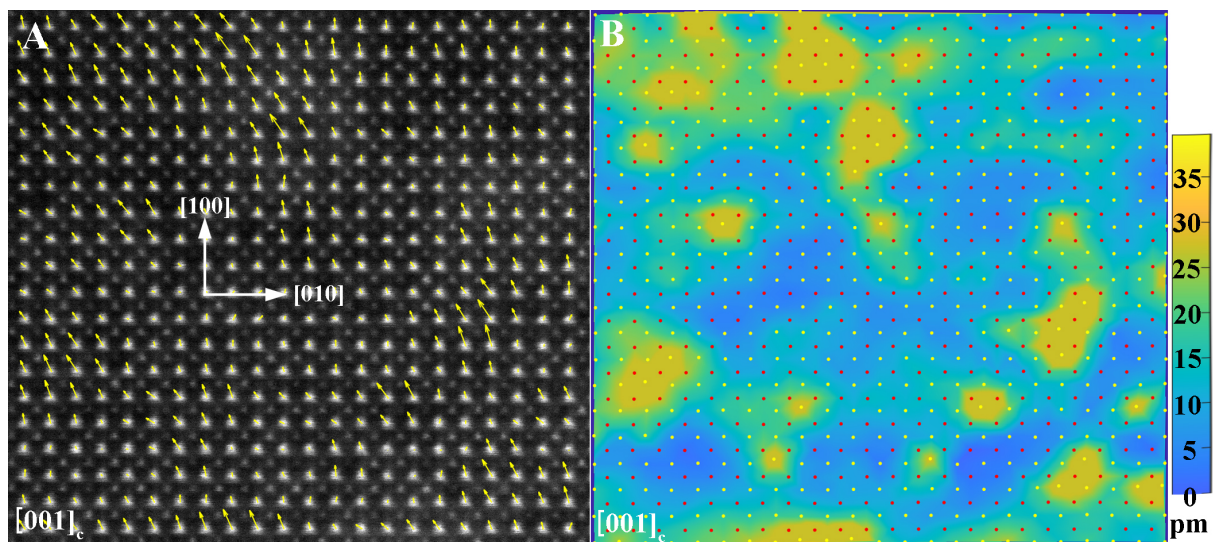


Figure 4. (A) Atomic-resolution HAADF-STEM polarization vector image and (B) polarization displacement distribution mappings along $[100]_c$.

repeatable double P-E loop, quite low energy efficiency can also be found owing to the large hysteresis caused by the first order antiferroelectric-ferroelectric phase transition. An obvious increase in both energy storage density and efficiency can be detected with the entrance of relaxor ferroelectric phase zone of $x > 0.1$, accompanied by the generation of slim P-E loops. Moreover, energy efficiency tends to increase with increasing relaxor behavior. Thus a good balance with both large W_{rec} and η can be commonly realized in superparaelectrics. [Figure 5A](#) shows the P-E loops and energy storage properties of 0.85NN-0.15CZ ceramic under various electric fields. It is found that P_{max} and P_r gradually increase when the electric field is applied from 2 kV/mm to 68 kV/mm, showing the characteristic of relaxor ferroelectric. As the electric field

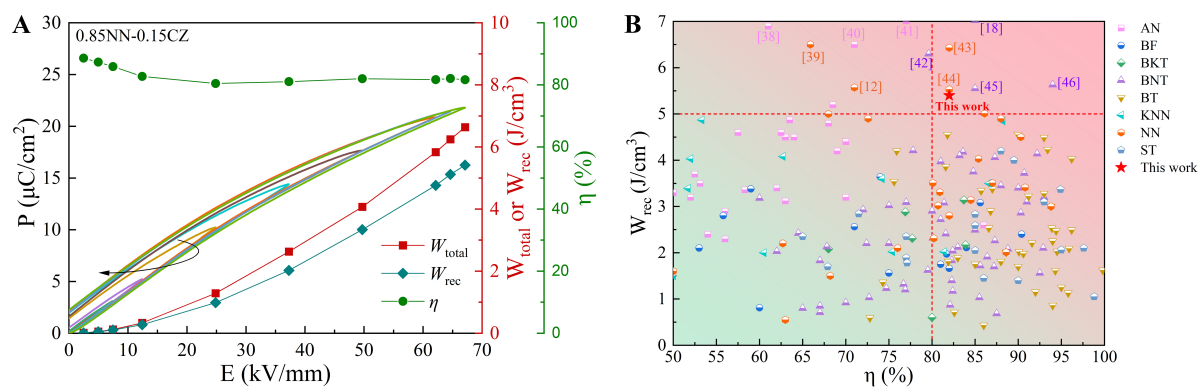


Figure 5. (A) P - E loops and energy storage performance under various electric fields for 0.85NN-0.15CZ ceramics. (B) Comparison of energy storage performance among 0.85NN-0.15CZ ceramic and some other systems^[6].

increases, W_{total} and W_{rec} present an almost parabolic growth trend. Eventually, a comprehensive performance of $W_{\text{rec}} \sim 5.4 \text{ J/cm}^3$ and $\eta \sim 82\%$ can be obtained in 0.85NN-0.15CZ ceramic under an ultrahigh external electric field of 68 kV/mm. It is believed that the excellent energy storage performance is associated with the following sections: Firstly, the sample with a small grain size of $\sim 2.1 \mu\text{m}$ has high grain boundary density, and the grain boundary with large resistance can act as a dissipative layer, effectively hindering the conduction of space charge and reducing the generation of leakage current. In addition, according to the relationship of $E_b \propto 1/\sqrt{G_a}$ ^[36], small grain size is favorable for the enhancement of E_b . Complex impedance spectroscopy of pure NN and 0.85NN-0.15CZ ceramics measured at 500 °C are shown in [Supplementary Figure 7](#). The Z'' - Z' curves of the two exhibited nearly a single semicircle arc with good fitting results using a series R||CPE equivalent circuit model, and 0.85NN-0.15CZ showed twice as much resistance as pure NN, which proves the dominant role to the enhanced E_b of the grain boundary. Secondly, the dense and uniform internal structure with few pores is beneficial to decreasing the possibility of local breakdown, which can broadly promote E_b ^[3]; Thirdly, the introduction of CZ induces the transition from antiferroelectric P phase to superparaelectric phase, leading to an enhanced relaxor behavior in ergodic relaxor region at room temperature. PNRs with fast electric field response characteristics can cause 0.85NN-0.15CZ ceramic to form the fast and reversible transition between relaxor ferroelectric and ferroelectric phase under an external electric field, resulting in a small P_r and a large η . Finally, 0.85NN-0.15CZ ceramic with moderate room-temperature ϵ_r can enhance W_{rec} by inhibiting early polarization saturation under external electric fields.

Advanced ceramic capacitors are developing toward large energy storage density and high efficiency^[37]. [Figure 5B](#) shows the comparison of energy-storage performance among 0.85NN-0.15CZ ceramic and other relevant dielectric energy storage ceramics (AgNbO_3 (AN), BiFeO_3 (BF), $\text{Bi}_{0.5}\text{K}_{0.5}\text{TiO}_3$ (BKT), $\text{Bi}_{0.5}\text{Na}_{0.5}\text{TiO}_3$ (BNT), BaTiO_3 (BT), $\text{K}_{0.5}\text{Na}_{0.5}\text{NbO}_3$ (KNN), SrTiO_3 (ST))^[6,12,18,38-46]. Obviously, 0.85NN-0.15CZ ceramic exhibits great performance superiority, making it one of the prospective materials for advanced pulse power capacitor applications.

CONCLUSIONS

In this work, $(1-x)\text{NN}-x\text{CZ}$ ceramics are prepared by a conventional solid-state reaction method. With increasing CZ content to 0.15, the structure of samples changes from antiferroelectric P phase to relaxor ferroelectric Q phase with superparaelectric state, leading to the destruction of long-range polarization ordering but reservation of antiferrodistortion ordering, which can be confirmed by the high energy synchrotron XRD and powder neutron diffraction refinement results as well as TEM images. In this case,

the grain size of the sample decreases to 2.1 μm , accompanied by dense and homogeneous microstructure. The 0.85NN-0.15CZ ceramics showed comprehensive energy storage performance of $W_{\text{rec}} = 5.4 \text{ J/cm}^3$ and $\eta = 82\%$ under an ultrahigh breakdown electric field of 68 kV/mm. The excellent energy storage performance is believed to originate from the small grain size, dense and homogeneous microstructure, superparaelectric state with fast polarization response, and delayed polarization saturation relating to the large oxygen octahedron tilt. The results of this work indicate that 0.85NN-0.15CZ ceramics exhibit colossal application potential in the field of dielectric energy storage.

DECLARATIONS

Authors' contributions

Experiment, characterization, writing original draft: Liu G

Review & editing, supervision: Qi H, Chen L

Conceptualization, review, supervision: Qi H

Availability of data and materials

Not applicable.

Financial support and sponsorship

This work was supported by the National Natural Science Foundation of China (Grant Nos. 52172181 and 22105017).

Conflicts of interest

All authors declared that there are no conflicts of interest.

Ethical approval and consent to participate

Not applicable.

Consent for publication

Not applicable.

Copyright

© The Author(s) 2023.

REFERENCES

1. Hao X, Zhai J, Kong LB, Xu Z. A comprehensive review on the progress of lead zirconate-based antiferroelectric materials. *Prog Mater Sci* 2014;63:1-57. [DOI](#)
2. Qi H, Xie A, Zuo R. Local structure engineered lead-free ferroic dielectrics for superior energy-storage capacitors: a review. *Energy Stor Mater* 2022;45:541-67. [DOI](#)
3. Yang L, Kong X, Li F, et al. Perovskite lead-free dielectrics for energy storage applications. *Prog Mater Sci* 2019;102:72-108. [DOI](#)
4. Wang G, Lu Z, Li Y, et al. Electroceramics for high-energy density capacitors: current status and future perspectives. *Chem Rev* 2021;121:6124-72. [DOI](#) [PubMed](#) [PMC](#)
5. Li J, Shen Z, Chen X, et al. Grain-orientation-engineered multilayer ceramic capacitors for energy storage applications. *Nat Mater* 2020;19:999-1005. [DOI](#) [PubMed](#)
6. Yang Z, Du H, Jin L, Poelman D. High-performance lead-free bulk ceramics for electrical energy storage applications: design strategies and challenges. *J Mater Chem A* 2021;9:18026-85. [DOI](#)
7. Yao FZ, Yuan Q, Wang Q, Wang H. Multiscale structural engineering of dielectric ceramics for energy storage applications: from bulk to thin films. *Nanoscale* 2020;12:17165-84. [DOI](#) [PubMed](#)
8. Veerapandiyam V, Benes F, Gindel T, Deluca M. Strategies to improve the energy storage properties of perovskite lead-free relaxor ferroelectrics: a review. *Materials* 2020;13:5742. [DOI](#) [PubMed](#) [PMC](#)
9. Guo X, Pu Y, Wang W, et al. Ultrahigh energy storage performance and fast charge-discharge capability in Dy- modified SrTiO₃ linear ceramics with high optical transmissivity by defect and interface engineering. *Ceram Int* 2020;46:21719-27. [DOI](#)

10. Xie A, Qi H, Zuo R, Tian A, Chen J, Zhang S. An environmentally-benign NaNbO₃ based perovskite antiferroelectric alternative to traditional lead-based counterparts. *J Mater Chem C* 2019;7:15153-61. DOI
11. Dong X, Li X, Chen X, et al. High energy storage density and power density achieved simultaneously in NaNbO₃-based lead-free ceramics via antiferroelectricity enhancement. *J Mater Sci* 2021;7:629-39. DOI
12. Tian A, Zuo R, Qi H, Shi M. Large energy-storage density in transition-metal oxide modified NaNbO₃-Bi(Mg_{0.5}Ti_{0.5})O₃ lead-free ceramics through regulating the antiferroelectric phase structure. *J Mater Chem A* 2020;8:8352-9. DOI
13. Bokov AA, Ye Z. Dielectric relaxation in relaxor ferroelectrics. *J Adv Dielectr* 2012;2:1241010. DOI
14. Cross LE. Relaxor ferroelectrics. *Ferroelectrics* 1987;76:241-67. DOI
15. Pan H, Lan S, Xu S, et al. Ultrahigh energy storage in superparaelectric relaxor ferroelectrics. *Science* 2021;374:100-104. DOI
16. Chen L, Wang N, Zhang Z, et al. Local diverse polarization optimized comprehensive energy-storage performance in lead-free superparaelectric. *Adv Mater* 2022;34:e2205787. DOI
17. Yang W, Zeng H, Yan F, et al. Superior energy storage properties in NaNbO₃-based ceramics via synergistically optimizing domain and band structures. *J Mater Chem A* 2022;10:11613-24. DOI
18. Qi H, Zuo R. Linear-like lead-free relaxor antiferroelectric (Bi_{0.5}Na_{0.5})TiO₃-NaNbO₃ with giant energy-storage density/efficiency and super stability against temperature and frequency. *J Mater Chem A* 2019;7:3971-8. DOI
19. Ye H, Yang F, Pan Z, et al. Significantly improvement of comprehensive energy storage performances with lead-free relaxor ferroelectric ceramics for high-temperature capacitors applications. *Acta Mater* 2021;203:116484. DOI
20. Kang R, Wang Z, Lou X, et al. Energy storage performance of Bi_{0.5}Na_{0.5}TiO₃-based relaxor ferroelectric ceramics with superior temperature stability under low electric fields. *Chem Eng J* 2021;410:128376. DOI
21. Glazer AM, Megaw HD. Studies of the lattice parameters and domains in the phase transitions of NaNbO₃. *Acta Crystallogr A* 1973;29:489-95. DOI
22. Megaw HD. The seven phases of sodium niobate. *Ferroelectrics* 1974;7:87-9. DOI
23. Megaw HD, Wells M. The space group of NaNbO₃ and (Na_{0.995}K_{0.005})NbO₃. *Acta Crystallogr* 1958;11:858-62. DOI
24. Guo H, Shimizu H, Mizuno Y, Randall CA. Strategy for stabilization of the antiferroelectric phase (Pbma) over the metastable ferroelectric phase (P2₁ma) to establish double loop hysteresis in lead-free (1-x)NaNbO₃-xSrZrO₃ solid solution. *J Appl Phys* 2015;117:214103. DOI
25. Qi H, Zuo R, Xie A, et al. Ultrahigh energy-storage density in NaNbO₃-based lead-free relaxor antiferroelectric ceramics with nanoscale domains. *Adv Funct Mater* 2019;29:1903877. DOI
26. Guo H, Shimizu H, Randall CA. Direct evidence of an incommensurate phase in NaNbO₃ and its implication in NaNbO₃-based lead-free antiferroelectrics. *Appl Phys Lett* 2015;107:112904. DOI
27. Reznichenko LA, Shilkina LA, Gagarina ES, et al. Structural instabilities, incommensurate modulations and P and Q phases in sodium niobate in the temperature range 300-500 K. *Crystallogr Rep* 2003;48:448-56. DOI
28. Wang X, Shen Z, Hu Z, Qin L, Tang S, Kuok M. High temperature Raman study of phase transitions in antiferroelectric NaNbO₃. *J Mol Struct* 1996;385:1-6. DOI
29. Bokov AA, Ye Z. Recent progress in relaxor ferroelectrics with perovskite structure. *J Mater Sci* 2006;41:31-52. DOI
30. Hu Q, Tian Y, Zhu Q, et al. Achieve ultrahigh energy storage performance in BaTiO₃-Bi(Mg_{1/2}Ti_{1/2})O₃ relaxor ferroelectric ceramics via nano-scale polarization mismatch and reconstruction. *Nano Energy* 2020;67:104264. DOI
31. Yan F, Zhou X, He X, et al. Superior energy storage properties and excellent stability achieved in environment-friendly ferroelectrics via composition design strategy. *Nano Energy* 2020;75:105012. DOI
32. Glazer AM. Simple ways of determining perovskite structures. *Acta Crystallogr A* 1975;31:756-62. DOI
33. Guo H, Shimizu H, Randall CA. Microstructural evolution in NaNbO₃-based antiferroelectrics. *J Appl Phys* 2015;118:174107. DOI
34. Liu Z, Lu J, Mao Y, Ren P, Fan H. Energy storage properties of NaNbO₃-CaZrO₃ ceramics with coexistence of ferroelectric and antiferroelectric phases. *J Eur Ceram Soc* 2018;38:4939-45. DOI
35. Shimizu H, Guo H, Reyes-Lillo SE, Mizuno Y, Rabe KM, Randall CA. Lead-free antiferroelectric: xCaZrO₃-(1-x)NaNbO₃ system (0 ≤ x ≤ 0.10). *Dalton Trans* 2015;44:10763-72. DOI
36. Tunkasiri T, Rujijanagul G. Dielectric strength of fine grained barium titanate ceramics. *J Mater Sci Lett* 1996;15:1767-9. DOI
37. Luo N, Han K, Cabral MJ, et al. Constructing phase boundary in AgNbO₃ antiferroelectrics: pathway simultaneously achieving high energy density and efficiency. *Nat Commun* 2020;11:4824. DOI
38. Chao W, Gao J, Yang T, Li Y. Excellent energy storage performance in La and Ta co-doped AgNbO₃ antiferroelectric ceramics. *J Eur Ceram Soc* 2021;41:7670-7. DOI
39. Chen J, Qi H, Zuo R. Realizing Stable Relaxor Antiferroelectric and Superior Energy Storage Properties in (Na_{1-x/2}La_{x/2})(Nb_{1-x}Ti_x)O₃ Lead-Free Ceramics through A/B-Site Complex Substitution. *ACS Appl Mater Interfaces* 2020;12:32871-9. DOI
40. Lu Z, Bao W, Wang G, et al. Mechanism of enhanced energy storage density in AgNbO₃-based lead-free antiferroelectrics. *Nano Energy* 2021;79:105423. DOI
41. Li S, Hu T, Nie H, et al. Giant energy density and high efficiency achieved in silver niobate-based lead-free antiferroelectric ceramic capacitors via domain engineering. *Energy Stor Mater* 2021;34:417-26. DOI
42. Guo B, Yan Y, Tang M, et al. Energy storage performance of Na_{0.5}Bi_{0.5}TiO₃ based lead-free ferroelectric ceramics prepared via non-uniform phase structure modification and rolling process. *Chem Eng J* 2021;420:130475. DOI
43. Chen H, Shi J, Dong X, et al. Enhanced thermal and frequency stability and decent fatigue endurance in lead-free NaNbO₃-based

- ceramics with high energy storage density and efficiency. *J Materiomics* 2022;8:489-97. DOI
44. Pang F, Chen X, Sun C, et al. Ultrahigh energy storage characteristics of sodium niobate-based ceramics by introducing a local random field. *ACS Sustain Chem Eng* 2020;8:14985-95. DOI
 45. Zhu C, Cai Z, Luo B, et al. Multiphase engineered BNT-based ceramics with simultaneous high polarization and superior breakdown strength for energy storage applications. *ACS Appl Mater Interfaces* 2021;13:28484-92. DOI
 46. Yan F, Huang K, Jiang T, et al. Significantly enhanced energy storage density and efficiency of BNT-based perovskite ceramics via A-site defect engineering. *Energy Stor Mater* 2020;30:392-400. DOI